Plasmon-induced enhancement of nonlinear optical processes in a double-resonant metallic nanostructure grating

Noordam, M. L.; Hernandez-Rueda, J.; Talsma, L. Y.; Kuipers, L.

DOI
10.1063/1.5141408

Publication date
2020

Document Version
Accepted author manuscript

Published in
Applied Physics Letters

Plasmon-Induced Enhancement of Nonlinear Optical Processes in a Double-Resonant Metallic Nanostructure Grating

M. L. Noordam,[1] J. Hernandez-Rueda,[1] L. Y. Talsma,[1] and L. Kuipers[1, a)]
Kavli Institute of Nanoscience Delft, Department of Quantum Nanoscience, Delft University of Technology, Lorentzweg 1, 2628 CJ Delft, The Netherlands

(Dated: 1 April 2020)

Nanostructured gratings in a metal surface can highly enhance nonlinear optical processes. The geometrical parameters that characterize a grating can be optimized to achieve intense near-fields, which in turn enhance the nonlinear optical signals. For a nonlinear process that involves multiple frequencies, like four-wave mixing (FWM), the optimization of grating parameters necessary to enhance the radiation incoupling for both frequencies is not trivial. Here we propose, compute and experimentally demonstrate a grating design that is resonant to two excitation frequencies and thus enhances the frequency mixing processes more efficiently. Second- and third-order nonlinear mechanisms are studied using two spatially and temporally overlapped laser pulses with different frequencies. Using our grating design we achieve an unprecedented nonlinear FWM enhancement factor of 7×10^3.

Since the first demonstration of second harmonic generation (SHG) in 1961[1], nonlinear optics has been studied extensively in a variety of materials. In particular, crystals have often been used to generate and investigate nonlinear effects due to their high nonlinear coefficients and wide frequency range of transparency. More recently, the optical response of metal/dielectric interfaces has attracted attention in the field of nanophotonics[2]. The highly localized nature of physical mechanisms at the surface of a metal typically leads to a lower nonlinear optical response than the one observed in nonlinear crystals resulting from a significantly reduced nonlinear interaction length. However, the nonlinear optical signals from a metal/dielectric interface can be greatly enhanced by employing nanostructures such as periodic arrays of cavities[3–5] or gratings[6,7] on a metal surface. When the geometrical parameters of such nanostructures match the wavelength of the incoming light plasmonic resonances can greatly enhance the local electric field near the surface increasing the nonlinear response[8,9]. Due to the sensitivity of the nonlinear signal on the geometric properties nonlinear optics on a surface can be functionalized to probe nanoparticles[10,11] or can be used for biosensing applications[12].

Various nonlinear optical effects that occur on a nanostructured gold film as a result of illuminating it with incident laser beams at two frequencies ω_1 and ω_2 include: SHG, $2\omega_1$ and $2\omega_2$, sum-frequency generation (SFG), $\omega_1+\omega_2$, third harmonic generation (THG), $3\omega_1$ and $3\omega_2$ and FWM, $2\omega_1-\omega_2$ and $2\omega_2-\omega_1$. These nonlinear effects can be described using the expansion of the nonlinear polarization up to third order,

$$\mathrm{P}_i = \varepsilon_0 \left[\sum_j \chi^{(1)}_{ij} \mathrm{E}_j + \sum_{jk} \chi^{(2)}_{ijk} \mathrm{E}_j \mathrm{E}_k + \sum_{jkl} \chi^{(3)}_{ijkl} \mathrm{E}_j \mathrm{E}_k \mathrm{E}_l \right], \quad (1)$$

where E_n is the n^{th} component of the electric field vector associated with the incoming laser beams illuminating the gold film, ε_0 is the vacuum permittivity and $\chi^{(m)}$ is the m^{th}-order susceptibility, which is a tensor of rank $m+1$. The second (third) term on the right-hand side of eq. 1 corresponds to the second (third) order nonlinear polarization. From equation 1 it follows that the nonlinear polarization vector scales with incoming electric fields of the nonlinear process, e.g. the SHG nonlinear signal scales quadratically with the incoming electric field, while the FWM nonlinear signal depends on electric fields with two different frequencies and scales quadratically with one of them and linearly with the other.

It also follows from eq. 1 that the efficiency of nonlinear optical processes will increase strongly by enhancing the local electric field near the surface. Surface charge density oscillations at a metal/dielectric interface, often referred to as surface plasmons, exhibit high local electric fields near the interface. Therefore, coupling the incident light to surface plasmons will strongly enhance the electric near-field close to the metal surface[13]. A grating can be used to couple the incident laser light into different kinds of plasmons: localized surface plasmons (LSPs) and surface plasmon polaritons (SPPs)[14,15]. First, we consider the coupling of the incoming laser light into LSP taking into account the geometry of an individual slit of the grating. The slits can be treated as a metal-insulator-metal cavity where the resonance condition depends on the depth and the width of the slits. Secondly, the coupling into the SPPs can be enhanced by optimizing the grating period. The coupling of the incident laser light into plasmon modes that results of illuminating a grating with laser light depends on the depth (d) and the width (w) of the individual slits and the grating period (Λ_g). Gratings that induce resonances have shown large enhanced FWM[7] and SHG[16] signals, when compared to the response of a flat metal interface.

The fact that the FWM generation efficiency depends on two laser frequencies makes the optimization of the grating parameters more intricate than for single-frequency based processes. Double-resonant enhancement of FWM processes have been shown in gold nano-antennas, which are resonant to the two frequencies of the incoming beams[17]. Also, double-resonant nanostructures have been demonstrated to enhance SHG, where the nanostructures are simultaneously resonant to the frequency of the incoming light and the frequency of the second harmonic[16,18,19]. The nanostructured gratings in the above-mentioned works were based on a geometry where

a)Corresponding author; Electronic mail: L.Kuipers@tudelft.nl

individual grating slits were simultaneously resonant to two different wavelengths. Next to experimental demonstrations of double-resonant structures also theoretical simulations of nonlinear optics in multi-resonant structures using 2D materials such as graphene shows promising results[20].

In this letter, we numerically compute and experimentally demonstrate a double-resonant plasmonic coupling via the enhancement of the FWM nonlinear optical process using a double-resonant nanostructure design where two gratings individually resonant to a single frequencies are combined, as depicted in Fig. 1(a). With finite-difference time-domain simulations (FDTD) simulations we study the near-field induced around the gratings using both laser frequencies. Using the simulations, we select optimal grating parameters to obtain a reliable nanostructure design that is fabricated with focused ion beam milling. We measure the nonlinear optical response of several gratings by using two laser pulses with different frequencies and observe FWM, SFG, SHG and THG nonlinear optical signals. We demonstrate the superior performance of the double-resonant grating on Au, reaching FWM yields three orders of magnitude larger than those measured at a flat air/Au interface. The FWM signals are readily observed by the naked eye.

For each sample a 200 nm gold layer was deposited on a glass slide using e-beam evaporation. The gratings are then etched into the thin gold film using focused ion beam milling (Helios, G4 CX DualBeam). A scanning electron microscope image of a machined sample is presented in Fig. 1(b) where the slits of alternating depth are clearly visible.

The optical nonlinear response of the nanostructured gratings is studied using the setup schematically depicted in Fig. 1(c). We use a femtosecond laser oscillator (Spectra-Physics, Tsunami) that generates pulses at a wavelength of 775 nm. With a pulse duration of roughly 150 fs and an optical parametric oscillator (Spectra-Physics, Opal) that delivers pulses at 1200 nm. A delay line is used to synchronize both beams before focusing onto the samples using an objective lens (Olympus UPlanSApo) to near-diffraction limited spot sizes of approximately 2 μm. The same objective lens is used to collect the generated nonlinear light. Due to a finite numerical aperture of the objective lens (NA = 0.95) the nonlinear light is detected up to a maximum angle (72°). To filter out the fundamental wavelengths while transmitting the nonlinear light, we use a dichroic mirror and two band-pass filters (Thorlabs, FGB37M). The spectra of the nonlinear light is recorded with a high-sensitivity cooled CCD-based spectrometer (SpectraPro 2300I).

Our double-resonant grating design combines two single-resonant gratings that are resonant for different frequencies. As shown in Eq.1, the nonlinear polarization is related to the electric field strength through the nonlinear susceptibility. In order to find the optimal single-resonant grating parameters, w, d and Λ_g for which the individual gratings are resonant, we simulate the electric field around the grating using FDTD simulation[7]. First, we find only a minute dependence on the slit width for all frequencies with a decaying local field enhancement for larger slit widths. Therefore, the slit width is chosen to be $w = 40$ nm for both single-resonant gratings,

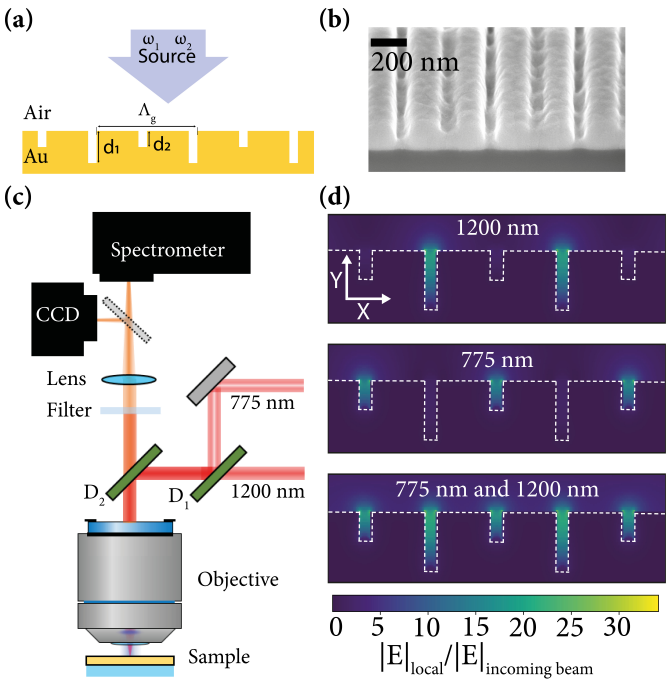

FIG. 1. (a) Illustration of the double-resonant grating nanostructures gold sample. (b) Scanning electron microscope image of a cross-cut of the double grating nanostructure taken at an angle of 52°. (c) Schematic of the optical setup. (d) Finite-difference time-domain simulations of the electric field, normalized to the electric field of the incoming beams. In the top map the double resonant grating structure is illuminated with a wavelength of 1200 nm and probed at 1200 nm. In the middle map the grating structure is illuminated with a wavelength of 775 nm and probed at 775 nm. In the bottom map we illuminated the grating with both the 775 nm and 1200 nm beams, the local field is evaluated separately at both wavelengths afterwards these two images are merged together.

the smallest slit width that can be fabricated in a reproducible manner. Secondly, we optimize the grating period and slit depth to maximize the near-field intensity as function of the frequency of the incoming light. The grating period is set to be equal for both single-resonant gratings to avoid some slits to overlap when the two gratings are combined. The grating period of $\Lambda_g = 470$ nm for both single-resonant gratings, is found to yield the optimal near-field enhancement upon 775 nm illumination. We choose the optimal value for the beam at 775 nm since its contribution to the FWM intensity scales quadratically with the laser intensity, while it scales linearly for the laser intensity at 1200 nm. Lastly, we optimize the slits depth where the simulations show a large influence on the near-field intensity for different laser frequencies. Due to this strong near-field dependence on the grating depth, the depth of the slits is set different for the two overlapping gratings. One grating has a depth of $d_1 = 75$ nm optimized for field enhancement at 775 nm and the other grating has a depth of $d_2 = 155$ nm optimized for field enhancement at 1200 nm.

After the optimisation of the grating parameters of the single-resonant gratings for different wavelengths, we simulate the near-field around the double-resonant grating, which

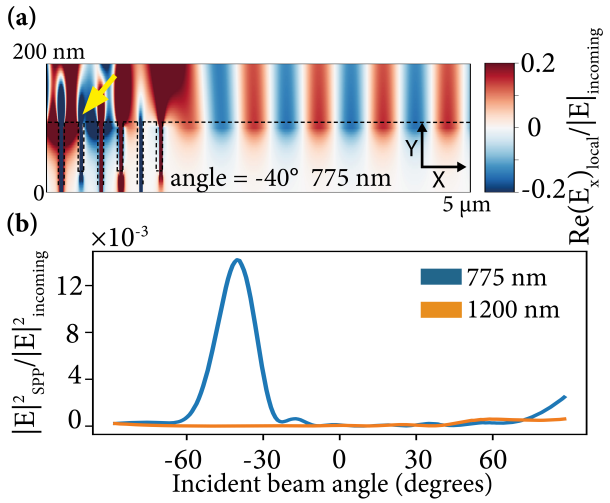

FIG. 2. (a) Finite-difference time-domain simulation of the real part of the x component of the electric field, normalized to the electric field of the incoming beam. The grating is excited with a wavelength of 775 nm at a -40° angle (indicated with arrow). (b) Normalized electric field as a function of incidence angle, determined 5 nm below the flat Au surface at 7.2μm from the edge of the grating at two incident wavelengths of of 775 nm (blue line) and 1200 nm (orange line) respectively.

is the result of overlapping the single-resonant gratings optimized for a wavelength of 1200 nm and 775 nm. Fig. 1(d) presents false color maps of the near-field enhancement factor, $\frac{|E|_{local}}{|E|_{incoming}}$, around the nanostructured gratings that we simulate using the FDTD method. When the double-resonant grating is illuminated only with the 1200 nm wavelength light source, we observe a local field enhancement (30×) in the 155 nm slits. For illumination with 775 nm, the local field enhancement (30×) occurs in the 75 nm slits. It should be noted that the off-resonant slits do not influence the local field enhancement of the resonant slits upon single wavelength excitation in the FDTD simulations. For example, when illuminating the double-resonant grating with only the 1200 nm light the local field enhancement in the resonant slits of $d_1 =$ 155 nm is the same when the $d_2 = 75$ nm slits are not present. Finally, when both beams illuminate the hybrid grating structure, the simulations show local field enhancement in both slits. This indicates that the designed grating can be used to optimize the in-coupling of both wavelengths in order to enhance the nonlinear response.

While the double-resonant grating is optimized for the coupling to LSPs it also couples the incident light into SPPs. A grating couples light into SPP's when, $k_{SPP} = k_{inc} + mG$. Here, $k_{inc} = k_0 sin(\theta)$ is the wavevector component of the incident light parallel to the electric field. $k_0 = \omega/c$ is the wavevector in vacuum and θ is the angle of the incident beam. $k_{SPP} = k_0\sqrt{\varepsilon_m(\omega)/(\varepsilon_m(\omega)+1)}$ is the wavevector of the SPPs, where $\varepsilon_m(\omega)$ is the real part of the dielectric constant of gold. m is an integer and $G = 2\pi/\Lambda_g$ is the wavevector of the grating. With $\Lambda_g = 470$ nm we calculate an angle

Enhancement	$d = 75$ nm and 155 nm	$d =$155 nm	$d =$75 nm
FWM	7302	1138	8.5
SFG	12	8.7	0.6

TABLE I. Nonlinear optical enhancement of FWM and SFG nonlinear optical processes for the double grating and individual gratings.

of incidence of -38.7° for an incoming wavelength of 775 nm, well below the maximum angle of our objective (72°). For an incoming wavelength of 1200 nm there is no real angle for which the wavevector equation holds. This means we can only excite SPPs of 775 nm wavelength with the double-resonant grating given the NA of the objective used. Fig. 2(a) presents false color map of the real part of the x component of the local electric field around the nanostructured grating that we simulate using the FDTD method. The grating is excited with 775 nm wavelength at an angle of -40°. This map illustrate the SSPs traveling on the gold surface when the double-resonant grating is illuminated under a -40° angle. In Fig. 2(b) we used a FDTD simulation varying the angle of the incident beam and probing the local electric field 5 nm below the surface, 7.2μm away from the grating. The simulation in Fig. 2(b) shows a peak at -40° for a 775 nm wavelength excitation and no peak for a 1200 nm wavelength excitation which is in good agreement with the calculated angles.

Fig. 3(a) depicts the spectra collected from plain gold and the double-resonant grating (note that the intensity is measured in electrical counts of the spectrometer). The peaks in the spectra can be assigned to the nonlinear optical signals corresponding to FWM (572 nm), SFG (472 nm), $SHG_{775\ nm}$ (388 nm) and $THG_{1200\ nm}$ (400 nm). These spectra demonstrate a clear enhancement of all nonlinear processes on the designed grating when compared to that of the flat gold surface. Fig. 3(b) presents the different signals as a function of the time-averaged (CW) power of the incident beams. The fact that in Fig. 3(b), we use a double logarithmic scale makes monomial functions appear as straight lines in the plot. The slopes of these lines correspond to the power order. To further illustrate that the different nonlinear effects scales with the same power as predicted by Eq. 1 we fitted the data with monomial functions of the first (orange lines), second (blue lines) and third (pink line) order. We observe a linear behaviour of the SFG signal and a quadratic behaviour of the FWM and $SHG_{775\ nm}$ signals as a function of the power of the 775 nm beam. Similarly, a linear behaviour of the FWM and SFG signals and a cubic behaviour of the $THG_{1200\ nm}$ signal are observed as a function of the power of the 1200 nm beam.

We investigate the nonlinear enhancements of both the single- and double-resonant gratings as depicted in the inset of Fig. 4. The spectra are presented in Fig. 4. The enhancement factors of the nonlinear processes are obtained by dividing the peak intensities by the one measured on a flat gold interface. These factors are listed in Table I. The single-resonant gratings exhibit FWM enhancement factors up to 1138 (d_1 = 155 nm) and 8.5 (d_2 = 75 nm). The double-resonant grating exhibits a remarkable enhancement factor of 7×10^3 for the

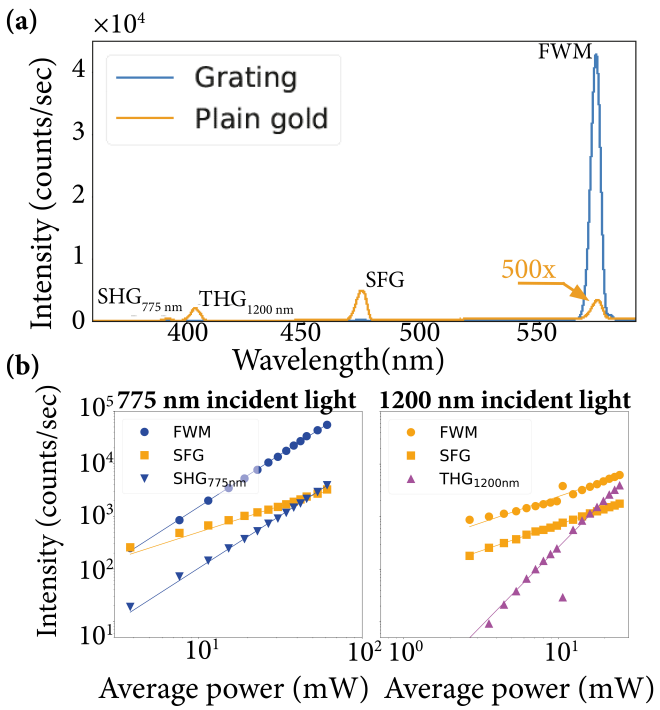

FIG. 3. (a) Spectra of the generated signal on a gold surface (orange) and the double nanostructure grating etched in gold (blue). $SHG_{775\ nm}$, $THG_{1200\ nm}$, SFG and FWM are observed on plain gold and the nanostructure. (b) Double logarithmic plot of the intensity of the nonlinear signals in gold as a function of the power of the incoming beams. The power functions of the nonlinear effects appear as straight lines on the double logarithmic scale where the slope corresponds to the power order of the nonlinear effect. Linear (orange), quadratic (blue) and cubic (pink) monomial functions are fitted through the data points.

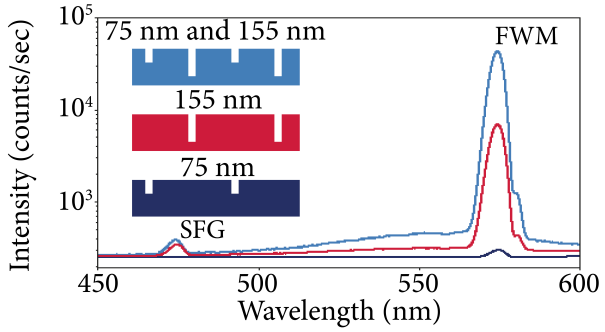

FIG. 4. Semi-log plot of the spectra for the double grating nanostructure and the individual gratings. The inset shows an illustration of the measured gratings.

FWM emission and an enhancement factor of 12 for the SFG emission. The observed enhancement in Table 1 demonstrates the superior performance of the double-resonant grating over the single-resonant gratings, as was expected from the near-field simulations using the FDTD method.

Furthermore, we measured the enhancement factors of the nonlinear processes depending on a single frequency i.e., $SHG_{775\ nm}$ and $THG_{1200\ nm}$, which are respectively 234 and 13 for the hybrid grating. Interestingly, these nonlinear processes also exhibit a higher enhancement using the hybrid grating. We also measured lower nonlinear enhancements in gratings with half of the period ($\Lambda_g = 235$ nm) and single slit depths (data not shown) to confirm that the large enhancement of the double-resonant grating is indeed not caused by the different grating period.

In contrast with previously studied double-resonant structures, our double-resonant grating enhances the incoming electric field at different spatial positions for the different frequencies. As a result, the overlap of the locally enhanced electric fields for the different frequencies is small. It is therefore not straightforward why the FWM and SFG nonlinear signals get enhanced by the double-resonant grating structure. Our results indicate an increased coupling to SPPs when the grating slits are resonant with the incoming wavelengths and that the nonlinear processes depending on two frequencies are mediated by the SPPs. Therefore the nonlinear enhancement of our double resonant grating structure is due generation of SPPs as well as LSPs. We will refer to the combination of LSPs as SPPs as surface plasmons.

To further illustrate and test the effect of the grating on the nonlinear processes we investigate the dependency of the FWM and SFG enhancement on the angle between the linear polarization vectors of the beams. Maximum enhancement is obtained when all incident polarization directions are perpendicular to the grooves. To underpin the plasmon-mediated nature of the nonlinear processes, we measure the FWM and SFG for different angles between the polarization direction of the incident beams, see fig. 5(a) and (b). Fig. 5(c) and (d) depict the FWM spectra collected from plain gold and from the double-resonant grating, respectively. Analogously, fig. 5(e) and (f) depict SFG spectra measured at the plain gold interface and at the double-resonant grating, respectively. The spectra are acquired for parallel (blue lines) or perpendicular (red lines) polarization directions. When illuminating plain gold with a perpendicular orientation between polarizations the resultant FWM signal is only a small fraction of the signal generated with a parallel orientation between polarizations as depicted in fig. 5(c). However, for the double-resonant grating the nonlinear signal of the perpendicular orientation between polarizations is almost the same as for the parallel orientation between polarizations, see fig. 5(d). The same amount of incident light is coupled into surface plasmons via the double-resonant grating because the electric field component perpendicular to the grating axis is the same for both polarization orientations. Therefore, the nonlinear signal generated by the surface plasmons do not decrease. The SFG on plain gold generated using the perpendicular orientation between polarizations illustrates that the nonlinear signal is roughly half of the nonlinear signal using the parallel orientation between polarizations, see fig. 5(e). Because of the centrosymmetry of the gold, the second-order nonlinear processes generated by the transverse component of the focused laser beams are very weak. Therefore, the second-order nonlinear signal generated by the longitudinal component of the tightly focused

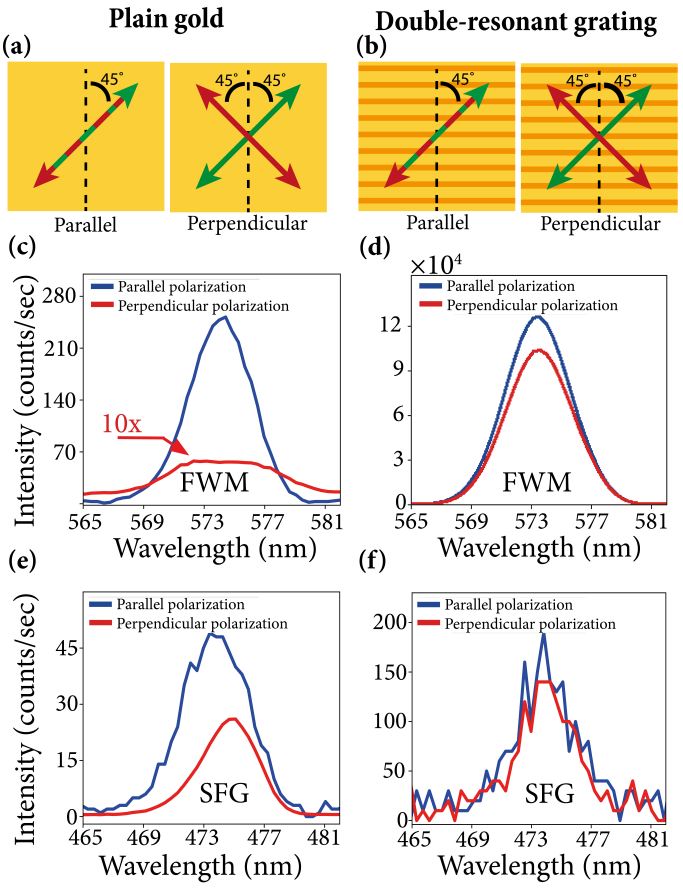

FIG. 5. Nonlinear optical responses of FWM and SFG where the polarization angles of the incident beams are parallel and perpendicular aligned. The polarization angles used for the parallel and perpendicular alignments are depicted in (a) on plain gold and in (b) on the double resonant grating. The green arrow depicts the polarization angle of the 775 nm incident light and the red arrow the polarization angle of the 1200 nm incident light. In (c) and (d) the FWM nonlinear signal is plotted when illuminating the plain gold and the double-resonant grating, respectively. In (e) and (g) the SFG nonlinear signal is plotted when illuminating the plain gold and the double-resonant grating, respectively.

laser beams, directed out of the gold film, is more dominant than the transverse component. The longitudinal component is not affected by the orientation between the polarizations of the incoming beams. Therefore, the SFG nonlinear signal is not affected as much as the FWM signal by the orientation between polarizations of the incoming beams. On the double-resonant grating the SFG nonlinear optical signal behaves the same way as the FWM signal for parallel and perpendicular orientation between polarizations alignments.

In conclusion we demonstrate enhancements of second- and third-order nonlinear effects depending on multiple frequencies using a double-resonant grating design. In this double-resonant grating two gratings with different slit depths optimized for two different frequencies are combined. Local electric field enhancements generated in the double-resonant grating induce surface plasmons that generate second- and third-order nonlinear enhancements of several orders of magnitude. For the FWM nonlinear signal depending on two different incoming frequencies we observe an enhancement of 7×10^3 in the double-resonant grating.

We thank Thomas Bauer and Irina Komen for their assistance in fabrication of nanostructured gold films. This work is part of the research program of the Netherlands Organization for Scientific Research (NWO). The authors acknowledge funding from the European Research Council (ERC Advanced Grant No. 340438-CONSTANS).

[1] P. A. Franken, A. E. Hill, C. Peters, and G. Weinreich, "Generation of Optical Harmonics," Phys. Rev. Lett. **7**, 118–120 (1961).
[2] Y. R. Shen, "Surface properties probed by second-harmonic and sum-frequency generation," Nature **337**, 519–525 (1989).
[3] J. A. H. Van Nieuwstadt, M. Sandtke, R. H. Harmsen, F. B. Segerink, J. C. Prangsma, S. Enoch, and L. Kuipers, "Strong modification of the nonlinear optical response of metallic subwavelength hole arrays," Phys. Rev. Lett. **97**, 146102 (2006).
[4] E. Almeida and Y. Prior, "Rational design of metallic nanocavities for resonantly enhanced four-wave mixing," Sci. Rep. **5**, 10033 (2015).
[5] R. Kolkowski, J. Szeszko, B. Dwir, E. Kapon, and J. Zyss, "Non-centrosymmetric plasmonic crystals for second-harmonic generation with controlled anisotropy and enhancement," Laser Photonics Rev. **10**, 287–298 (2016).
[6] J. Renger, R. Quidant, N. Van Hulst, and L. Novotny, "Surface-enhanced nonlinear four-wave mixing," Phys. Rev. Lett. **104**, 046803 (2010).
[7] P. Genevet, J. P. Tetienne, E. Gatzogiannis, R. Blanchard, M. A. Kats, M. O. Scully, and F. Capasso, "Large enhancement of nonlinear optical phenomena by plasmonic nanocavity gratings," Nano Lett. **10**, 4880–4883 (2010).
[8] M. Kauranen and A. V. Zayats, "Nonlinear plasmonics," Nat. Photonics **6**, 737–748 (2012).
[9] N. Panoiu, W. Sha, D. Lei, and G. Li, "Nonlinear optics in plasmonic nanostructures," J. Opt. **20**, 083001 (2018).
[10] Y. Jung, H. Chen, L. Tong, and J. X. Cheng, "Imaging gold nanorods by plasmon-resonance-enhanced four wave mixing," J. Phys. Chem. C **113**, 2657–2663 (2009).
[11] Y. Zhang, N. K. Grady, C. Ayala-Orozco, and N. J. Halas, "Three-dimensional nanostructures as highly efficient generators of second harmonic light," Nano Lett. **11**, 5519–5523 (2011).
[12] H. Aouani, O. Mahboub, N. Bonod, E. Devaux, E. Popov, H. Rigneault, T. W. Ebbesen, and J. Wenger, "Bright unidirectional fluorescence emission of molecules in a nanoaperture with plasmonic corrugations," Nano Lett. **11**, 637–644 (2011).
[13] L. Novotny and B. Hecht, "Principles of nano-optics," Cambridge university press (2012).
[14] H. Hagman, O. Bäcke, J. Kiskis, F. Svedberg, M. P. Jonsson, F. Höök, and A. Enejder, "Plasmon-enhanced four-wave mixing by nanoholes in thin gold films," Opt. Lett. **39**, 1001–1004 (2014).
[15] Y. Blechman, E. Almeida, B. Sain, and Y. Prior, "Optimizing the Nonlinear Optical Response of Plasmonic Metasurfaces," Nano Lett. **19**, 261–268 (2019).
[16] C. Y. Wang, H. Y. Chen, L. Sun, W. L. Chen, Y. M. Chang, H. Ahn, X. Li, and S. Gwo, "Giant colloidal silver crystals for low-loss linear and nonlinear plasmonics," Nat. Commun. **6**, 7734 (2015).
[17] H. Harutyunyan, G. Volpe, R. Quidant, and L. Novotny, "Enhancing the nonlinear optical response using multifrequency gold-nanowire antennas," Phys. Rev. Lett. **108**, 217403 (2012).
[18] Z. Zhu, B. Bai, H. Duan, H. Zhang, M. Zhang, O. You, Q. Li, Q. Tan, J. Wang, S. Fan, and G. Jin, "M-shaped grating by nanoimprinting: A replicable, large-area, highly active plasmonic surface-enhanced Raman scattering substrate with nanogaps," Small **10**, 1603–1611 (2014).
[19] S. Park, J. W. Hahn, and J. Y. Lee, "Doubly resonant metallic nanostructure for high conversion efficiency of second harmonic generation," Opt. Express **20**, 4856–4870 (2012).
[20] M. Weismann and N. C. Panoiu, "Theoretical and computational analysis of second-and third-harmonic generation in periodically patterned graphene and transition-metal dichalcogenide monolayers," Phys. Rev. B **94**, 035435 (2016).